Int. J. Electrochem. Sci., 17 **(2022)** Article Number: 220551, doi: 10.20964/2022.05.45

International Journal of
ELECTROCHEMICAL
SCIENCE
www.electrochemsci.org

Preparation of NiO Thin Films and Their Application for NO_2 Gas Detection

Guanglei Tan[1,], Dan Tang[2], Xiaomin Wang[1], Lijie He[1,*], Tao Mu[1], Gang Li[1]*

[1] Liaoning Key Laboratory of Chemical Additive Synthesis and Seperation, Yingkou Institute of Technology, Yingkou 115014, China;
[2] School of Mechanical Engineering, Yingkou Institute of Technology, Yingkou 115014, China
[*]E-mail: guangleitan1979@sina.com(Drs. *Guanglei Tan and Lijie He*)

Received: 2 February 2022 / *Accepted:* 16 March 2022 / *Published:* 5 April 2022

The current study reports the successful preparation of NiO thin films on the surface of a ceramic substrate using chemical spray pyrolysis, followed by their fabrication as NO_2 gas sensors. A 0.2 M nickel chloride solution was utilized for the purpose. We investigated the influence of different deposition times on the surface morphology, phase structure, optical transmittance, and NO_2 gas sensitivity of NiO thin films. The results suggested that, at a deposition time equal to 10 min, the NiO-10 thin film deposited by chemical spray pyrolysis presented a large number of honeycomb pores on the surface, thereby possessing a high specific surface area and porous structure (the porosity: ~5.6%). Among the four synthesized films, the NiO-10 thin film had the highest optical transmittance in the visible and near-infrared ranges. At an operating temperature of 200°C, the NiO-10, NiO-20, NiO-30, and NiO-40 thin film gas sensors had respective sensitivities of 57.8%, 53.3%, 40.5%, and 34.2%. Additionally, the NiO-10 thin film gas sensor demonstrated high stability and selectivity for sensing NO_2 gas. NiO-10 thin-film demonstrated a corrosion current density equal to 5.46×10^{-5} A/cm^2.

Keywords: NiO thin film; Deposition; Gas sensors; Microstructure; NO_2

1. INTRODUCTION

NO_2 is a toxic gas, which when inhaled by humans in increased concentration, causes lesions in the human respiratory system, thus seriously damaging human health [1-4]. Furthermore, the high concentration of NO_2 gas might toxify the surrounding environment [5]. Therefore, real-time detection of NO_2 gas has emerged as an important research area for the scientific community. Researchers are currently developing various types of gas sensors to detect NO_2 gas. Among the several sensors available, the most frequently used gas sensors are the metal oxide sensors, which offer high sensing

performance at a low cost and have advantages such as simple manufacturing, and high compatibility.

Nickel oxide (NiO), a unique p-type metal oxide semiconductor, is capable of forming thin films with excellent chemical and thermal stability and a wide direct band gap. Because the electrical properties of NiO are determined by the lattice defects of the Ni and O elements, NiO has a wide range of applications in electrochromism, manufacture of electrodes, and gas sensors [6-9]. Furthermore, NiO is unique in its ability to detect harmful gases. Several researchers have contributed significantly to the development of nickel oxide gas sensors in recent years. Kondrateva *et al.* [10] synthesized nickel oxide gas-sensitive nanomaterials through the citric acid method and characterized them using transmission electron microscopy (TEM) and X-ray diffraction (XRD). Zhao *et al.* [8] employed a sol-gel process to prepare NiO films and investigated their sensing properties for various gases. The findings demonstrated that NiO films might be employed as gas-sensitive materials in low-energy gas sensors. Zhao *et al.* [11] used the electrostatic spinning process to produce nickel oxide with a reticulated fiber structure and later fabricated it into a gas sensor. The gas sensor was discovered to have quick response characteristics to sensing gaseous acetone at a temperature of 250°C. There are numerous techniques for preparing NiO thin films, including magnetron sputtering, laser deposition, sol-gel method, chemical deposition, chemical spray pyrolysis, etc [12-15]. At appropriate temperature, Chemical spray pyrolysis can be used to prepare homogenous metal oxide layers, however, there are only a few studies on the preparation of NiO thin films by chemical spray pyrolysis. As a result, there is a growing need for research on different aspects related to the preparation of NiO thin films. The novel aspects of this work are as follows: (1) Four types of NiO thin films were prepared using the chemical spray pyrolysis method. (2) A sensor based on NiO thin film was fabricated for detecting NO_2 gas. (3) The surface morphology, organization, optical transmittance, and NO_2 gas sensitivity of NiO thin films were investigated in detail.

2. PREPARATION AND METHOD

2.1 Preparation

The NiO thin films were prepared on the surface of a ceramic substrate by chemical spray pyrolysis using 0.2 M nickel chloride solution ($NiCl_2$-$6H_2O$) as a raw material. The ceramic substrate was ultrasonically cleaned prior to the test, using a 200 W power, up to a cleaning time of 20 min. The substrate was then scrubbed with 75% acetone and alcohol. NiO thin films were prepared on a ceramic surface using CST-1 chemical spray pyrolysis equipment. The following parameters were used in the process: The temperature was maintained at 450°C, the oxygen pressure was set to 0.5 MPa, the deposition periods were set to 10 min, 20 min, 30 min, and 40 min, and then subsequently prepared samples were respectively labeled NiO-10, NiO-20, NiO-30, and NiO-40.

2.2 Characterization

The surface morphologies of NiO thin films were observed using a scanning electron microscope (SEM, S3400) and transmission electron microscope (TEM, JEM2100), respectively. A UV-3600 spectrophotometer was used to determine the optical transmittance of NiO thin films. Additionally,

D/Max-2400 X-ray diffraction (XRD) analyzer was used to examine the crystal structure of NiO thin films. The test conditions were as follows: Cu-K_α target (λ=0.154 nm), accelerating voltage 40 kV, tube current 100 mA, scanning step 0.05°, and scanning range 20°~90°. The NiO particle size (D) of NiO thin films was calculated using Scherer equation (1):

$$D = \frac{0.89\lambda}{\beta \cos\theta} \quad (1)$$

where D is the particle size of NiO, λ is the X-ray wavelength, β is the width of the sample diffraction peak at half height, and θ is the Bragg diffraction angle.

The ceramic sample of NiO thin films was cut and fabricated into a 10 mm×10 mm×5 mm NiO thin films gas sensor using the static gas distribution method. The gas sensitivity was determined using the WS-30A gas-sensitive element test device. Moreover, the sensitivity of the sensor was calculated by equation (2).

$$S = \frac{|R_a - R_g|}{R_a} \times 100\% \quad (2)$$

where S is the sensitivity of the sensor (%), Ra and Rg denote the sensor's resistance values in air and target gas (Ω), respectively.

A CS-350 electrochemical workstation (Wuhan Kesite Instruments Co., Ltd, Wuhan, PR China) was utilized to carry out a 2-hour electrochemical corrosion test of NiO thin films in a 3 wt.% NaCl liquid at a scan rate of 0.03 mV/s.

3. RESULTS AND DISCUSSION

3.1. Microstructure analysis

Fig. 1 presents the TEM image of NiO particles used for the preparation of NiO thin films. The black spots represent NiO particles, having an average size of 30.4 nm. As shown in the inset of Fig. 1, the electron diffraction (SAED) image of a selected area demonstrates that NiO thin films have a polycrystalline structure.

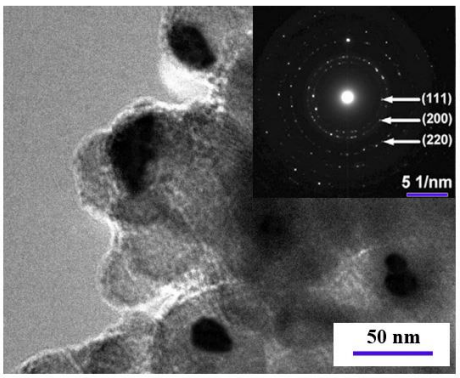

Figure 1. TEM image of NiO particles utilized for the preparation of thin films.

SEM images of NiO thin films prepared using chemical spray pyrolysis at various deposition time conditions are shown in Fig. 2. NiO-10, NiO-20, NiO-30, and NiO-40 thin films were found to be equally distributed over the ceramic surface, with no apparent cracks on their surface. However, when the deposition time was increased to 10 min, the surface of the NiO-10 thin-film manifested a considerable number of honeycomb pores, and the porosity was ~5.6%. As a result, the NiO-10 thin film had a large specific surface area and a porous structure, which facilitated NO_2 gas adsorption by NiO thin films. As illustrated in Figs. 1b and 1c, the pores in NiO-20 and NiO-30 thin films decreased dramatically as the deposition time was increased. The porosities of NiO-20 and NiO-30 films were 1.8% and 0.9%, respectively. When deposition time was 40 minutes, the NiO-40 thin film on the surface exhibited a denser organization structure and the lowest porosity (0.4%).

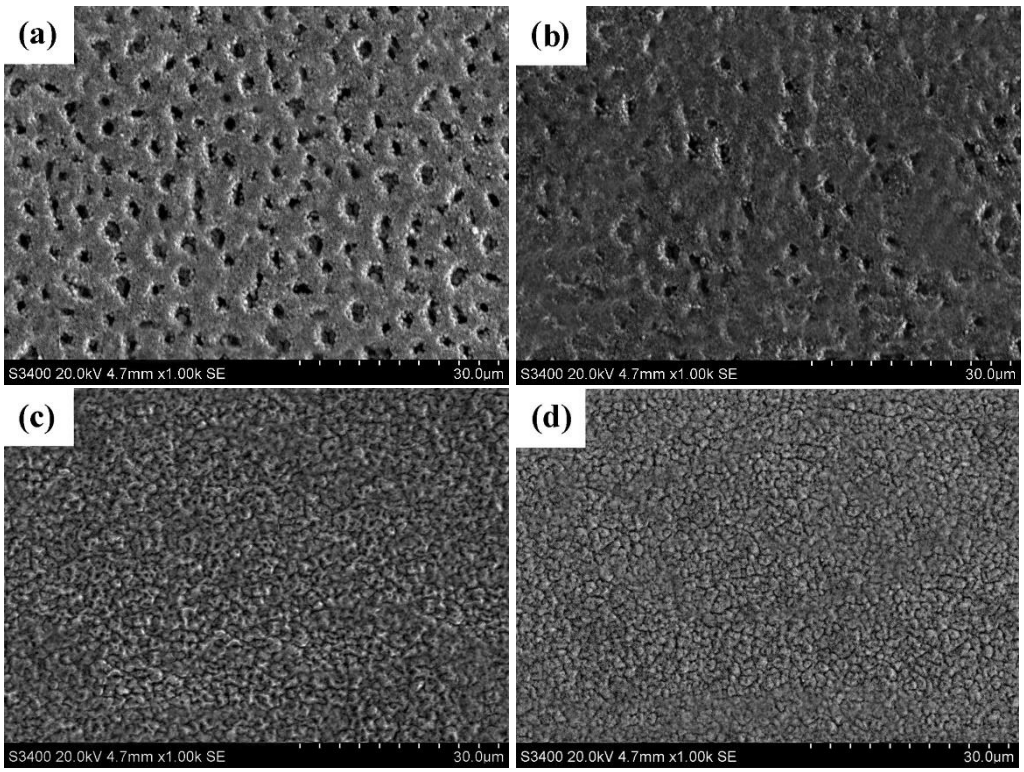

(a) NiO-10 film, (b) NiO-20 film, (c) NiO-30 film, (d) NiO-40 film

Figure 2. SEM images of NiO thin films obtained at various deposition times.

3.2 XRD test

The XRD patterns of NiO thin films prepared by chemical spray pyrolysis under various deposition time conditions have been shown in Fig. 3. The diffraction peaks of NiO-10, NiO-20, NiO-30, and NiO-40 thin films correspond to the (1 1 1), (2 0 0), and (2 2 0) lattice planes, respectively. According to the data of JCPDS No. 47-1049 and Fig. 3, the four NiO thin films were all NiO phases with a face-centered cubic structure that were created by the (1 1 1) crystal plane as the optimal orientation. Using Scheller's formula, the average particle size of the NiO particles in the thin films was

calculated to be about ~30 nm, which is in agreement with the TEM measurement.

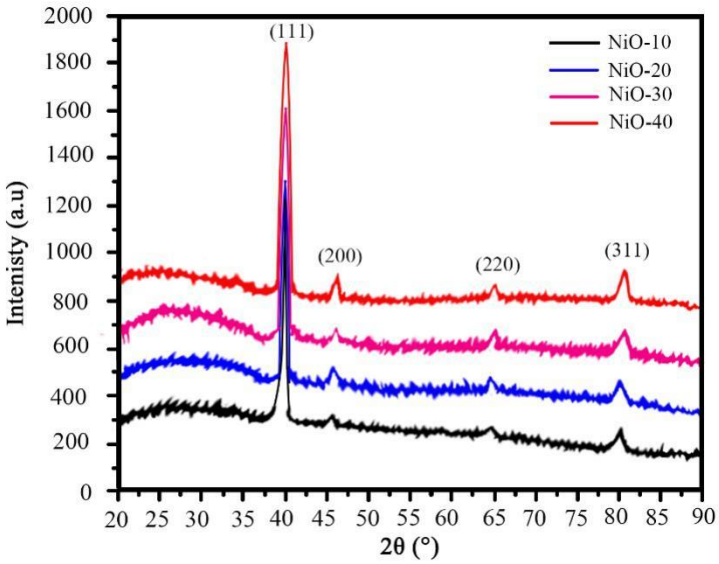

Figure 3. XRD patterns of NiO thin films prepared at various deposition times.

3.3 Optical transmittance

Fig. 4 depicts the transmittance curves of NiO thin films deposited using chemical spray pyrolysis under various deposition time conditions.

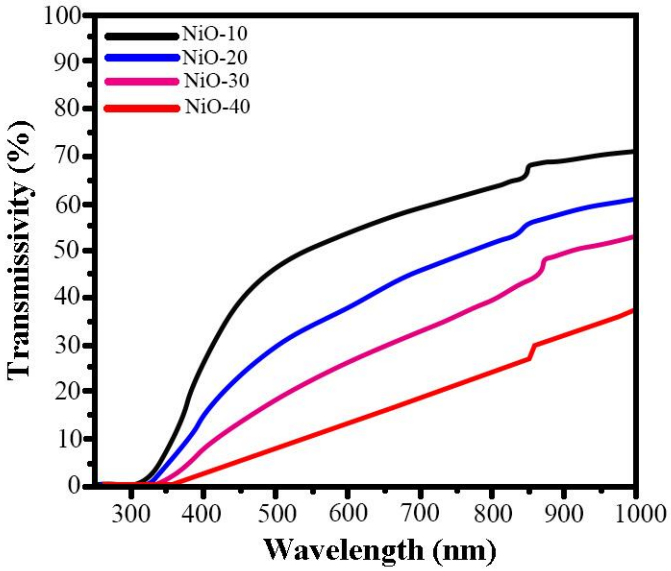

Figure 4. Transmittance curves of NiO thin films prepared at different deposition times.

As shown in Fig. 4a, NiO-10, NiO-20, NiO-30, and NiO-40 thin films manifested good transparencies in the visible and near-infrared regions. Furthermore, the four synthesized films displayed

higher absorption in the UV region ranging from 300-380 nm. In comparison to the other three films, the NiO-10 thin film exhibited the highest optical transmittance in the visible and near-infrared regions. The optical transmittance of NiO thin films decreased as the deposition time increased. The precise reason for this observation is the increase in thickness of NiO thin films with the increase of deposition time. The longer the deposition time during film preparation, the greater is the thickness of the deposited thin films and the greater is the density of their organization. Consequently, it becomes difficult for incident light to penetrate the NiO thin films, thereby reducing their transmittance [16].

3.4 Gas sensitivity

In general, under high temperatures conditions gas can be adsorbed by most metal oxide gas sensors [17, 18]. The gas sensitivity test for NO_2 gas at a concentration of 20 ppm was performed using the NiO thin film gas sensor, as shown in Fig. 5. The temperature during the investigation was maintained in the 100°C-250°C range. The sensitivity of the NiO thin film gas sensor to NO_2 gas increased rapidly as the operating temperature increased from 100°C to 200°C, reaching a maximum at 200°C. As NO_2 gas decomposes into oxygen and NO gas at high temperature, the amount of NO_2 particles adsorbed on the surface of the NiO thin film was reduced, hence increasing the sensitivity of the NiO thin film gas sensor [19]. However, the sensitivity of the NiO thin film gas sensor decreased when the operating temperature increased gradually from 200°C to 250°C. The reduced rate decomposition of NO_2 into oxygen and NO at high temperature led to a decrease in the sensitivity of the NiO thin film-based gas sensor.

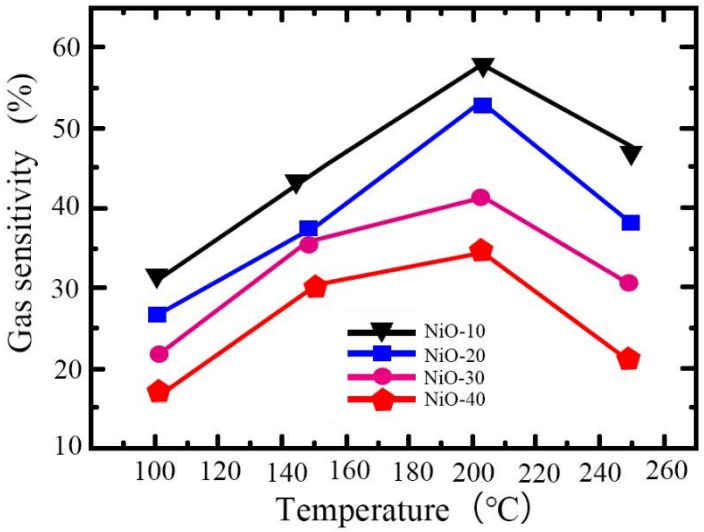

Figure 5. Effect of temperatures on the gas sensitivity of NiO thin films to NO_2 gas.

Additionally, Fig. 5 indicates that the NiO-10, NiO-20, NiO-30, and NiO-40 thin film gas sensors

had a sensitivity of 57.8%, 53.3%, 40.5%, and 34.2%, respectively, at 200°C operating temperature. Thus, the NiO-10 gas sensor demonstrated the highest gas sensitivity at 200°C, which can be attributed to the high crystallinity of the NiO-10 thin film, a substantial number of oxygen vacancies, as well as the honeycomb-like surface morphology of the film [20]. Table 1 presents the gas sensitivities of NiO thin film gas sensors compared with the literature reported by Gomaa *et al.* [8]. It was obvious that the gas sensitivity of NiO-10 film was higher than that of NiO-5 min obtained by Gomaa *et al.*

Table 1. Comparison results of the gas sensitivities of NiO thin film gas sensors.

Our samples	Gas sensitivity (%)	Sample [20]	Gas sensitivity (%)
NiO-10	57.8	NiO-5 min	57.3
NiO-20	53.3	NiO-10 min	53
NiO-30	40.5	NiO-15 min	41
NiO-40	34.2	NiO-20 min	35

Gas sensors must be highly selective and stable during their manufacturing [21]. The NiO-10 thin film gas sensor was tested for its sensitivity against acetone, carbon monoxide, carbon dioxide, sulfur dioxide, and NO_2 gases, respectively, as shown in Fig. 6.

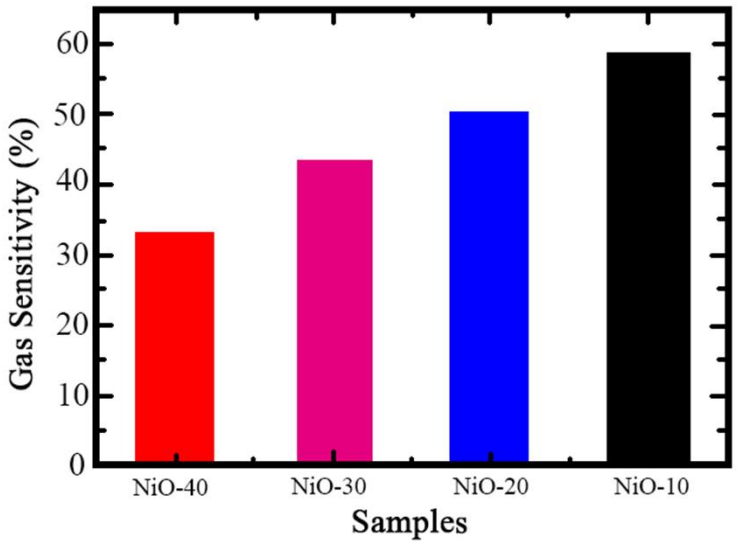

Figure 6. Histogram of selectivity of NiO thin film gas sensors in 20 ppm gas concentration

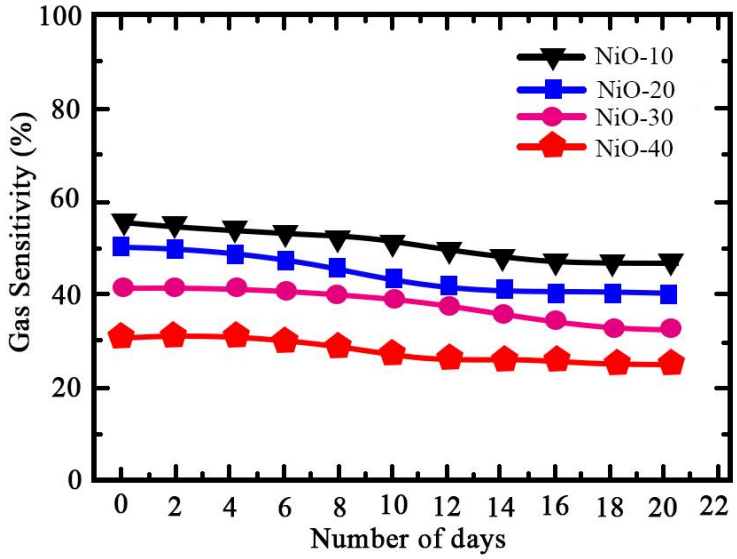

Figure 7. Stability curves of NiO thin film gas sensors

The NiO thin film gas sensor displayed a low sensitivity towards acetone, CO_2, SO_2, and CO gases, as presented in Fig. 6. On the other hand, the sensitivity of the NiO thin film-based gas sensor to NO_2 gas was extremely high, thereby implying that the NiO thin film gas sensor possessed a high selectivity for NO_2 gas. It was noteworthy that the NiO-10 sensor had the maximum gas sensitivity of 57.8% among all four gas sensors.

In an attempt to determine their stabilities, NiO thin film gas sensors were subjected to a stability test over the length of 20 days, as illustrated in Fig. 7. The gas sensitivities of the four sensors gradually decreased as the test time increased from 1 to 16 days. The existence of moisture or oxide layers on the sensor surface led to some changes in the gas sensitivities of the sensors. Additionally, the gas sensitivities of all sensors changed only minimally, thereby suggesting that the sensor material has good stability. Notably, of the four gas sensors tested, the NiO-10 thin film gas sensor manifested the highest selectivity and stability towards NO_2.

3.5 Polarization curves of NiO thin films

In order to examine the corrosion resistance of the NiO thin films in a wet environment, the electrochemical corrosion test was carried out in a 3 wt.% NaCl liquid. The potentiodynamic polarization curves for NiO thin films have been illustrated in Figure 8. Based on Figure 8, Table 2 presents electrochemical parameters for NiO thin films. NiO-10, NiO-20, NiO-30, and NiO-40 thin films demonstrated respective corrosion potentials of -0.551, -0.468, -0.443, and -0.312 V. Furthermore, NiO-10 thin-film demonstrated a corrosion current density of 5.46×10^{-5} A/cm^2, which was the largest amongst all the films. The results indicated that the NiO-10 thin film had a large specific surface area and a porous structure, which resulted in the NaCl liquid easily into the film interior. As a result, the corrosion potential of NiO-10 film was the largest among all four films, illustrating a poor corrosion resistance.

The outcomes corroborate quite well with the work of Ma *et al.* [22].

It was obvious that higher porosity of the NiO-10 thin film caused a higher corrosion current density (5.46×10^{-5} A/cm^2) during the electrochemical corrosion test. While the gas sensitivity of the film was the highest among all thin films. The results indicated that a shorter the deposition time, the larger is the porosity of the deposited thin films. Thus, the film was difficult to prevent the NaCl corrosion solution from dipping into the film. Therefore, the corrosion potential of NiO-10 film was the largest among all coatings. In addition, the gas sensitivities of NiO-20, NiO-30 and NiO-40 films were 53.3%, 40.5% and 34.2%, while the corrosion current densities were 4.65×10^{-5}, 3.51×10^{-5}, and 2.21×10^{-5} A/cm^2, respectively. Therefore, to ensure the gas sensitivities and service life of NiO thin films, the NiO-10 gas sensor should not be applied in humid environments.

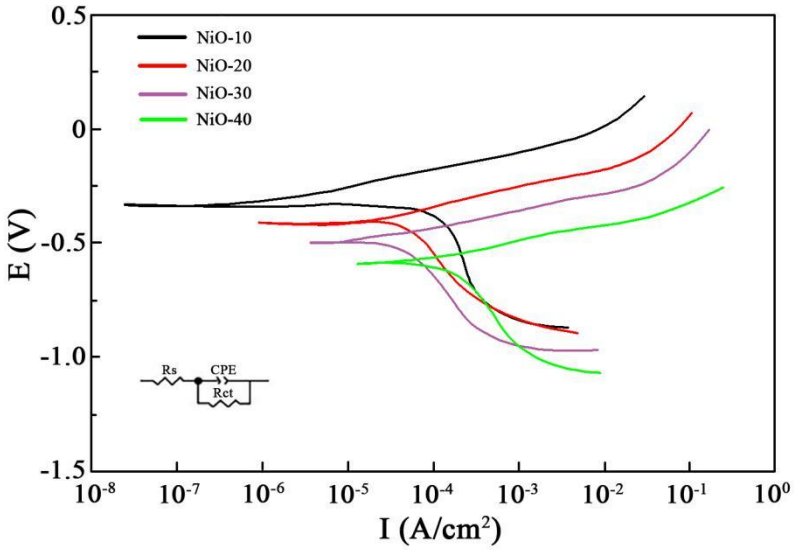

Figure 8. Polarization curves for the NiO thin films at 3 wt.% NaCl liquid and 0.03 mV/s scan rate.

Table 2. Electrochemical parameters for NiO thin films at 3 wt.% NaCl liquid and 0.03 mV/s scan rate.

Thin films	NiO-10	NiO-20	NiO-30	NiO-40
β_a (V/dec)	0.043	0.021	0.023	0.024
β_c (V/dec)	0.032	0.031	0.033	0.035
R (Ω/cm^2)	2547	3937	6864	6949
E (V)	−0.551	−0.468	−0.443	−0.312
I (A/cm^2)	5.46×10^{-5}	4.65×10^{-5}	3.51×10^{-5}	2.21×10^{-5}

4. CONCLUSION

(1) NiO thin films were prepared on the surface of a ceramic substrate using chemical spray pyrolysis and subsequently employed to fabricate NO_2 gas sensors. Among these, the NiO-10 thin film exhibited a substantial number of honeycomb pores on the surface, following 10 min of deposition. As a result, the NiO-10 thin film had a high specific surface area and a porous structure, and the porosity was ~5.6%.

(2) The diffraction peaks of prepared NiO-10, NiO-20, NiO-30, and NiO-40 thin films were found to correspond to the lattice planes of (1 1 1), (2 0 0), and (2 2 0), respectively. Furthermore, the four synthesized films exhibited a face-centered cubic structure of the nickel oxide phase, with NiO particles having an average particle diameter of 30-42 nm. The NiO-10 thin-film demonstrated the highest optical transmittance in the visible and near-infrared ranges when compared to the other three films.

(3) The sensitivity of the NiO thin film gas sensor to NO_2 gas increased rapidly as the operating temperature increased from 100°C to 200°C. At an operating temperature of 200°C, the NiO-10, NiO-20, NiO-30, and NiO-40 thin film gas sensors respectively manifested a sensitivity of 57.8%, 53.3%, 40.5%, and 34.2%. Furthermore, of the four gas sensors tested, the NiO-10 thin film gas sensor demonstrated the highest stability and selectivity towards NO_2 gas. Besides, NiO-10 thin film exhibited a corrosion current density equivalent to 5.46×10^{-5} A/cm^2.

ACKNOWLEDGEMENT
The finance support provided by Liaoning Key Laboratory of Chemical Additive Synthesis and Seperation (ZJNK2016), General project of Education Department of Liaoning Province（LJKZ1196）, Liaoning Provincial Education Department scientific Research Project（L2019010）, Excellent Talents of Science and Technology in Yingkou Institute of Technology (RC201903), Innovative Research Team in Yingkou Institute of Technology (TD201901), Innovative Research Team in Yingkou Institute of Technology（TD202001）.

References

1. Y. Wang, L. Yao, L. Xu, W. Wu, W. Lin, C. Zheng, Y. Feng, and X. Gao, *Sens. Actuators. B: Chem.*, 332 (2021) 129497.
2. T. Zhang, J. Dong, Y. Ji, D. Kong, and J. Lu, *Sci. Total. Environ.*, 802 (2022) 149850.
3. C. Balamurugan, S.J. Song, and H.S. Kim, J. *Korean. Ceram. Soc.*, 55 (2018) 1-20.
4. R.R. Kumar, T. Murugesan, T.W. Chang, and H.N. Lin, *Mater. Lett.*, 287 (2021) 129257.
5. D. Galán-Madruga and J.P. García-Cambero, *J. Environ. Sci*., 111 (2022) 164-174.
6. S.M. Majhi, A. Mirzaei, H.W. Kim, S.S. Kim, and T.W. Kim, *Nano. Energy.,* 79 (2021) 105369.
7. F. Xia, C. Li, C. Ma, Q. Li, and H. Xing, *Appl. Surf. Sci.*, 538 (2021) 148139.
8. M.M. Gomaa, M.H. Sayed, E. Chikoidze, Y. Dumont, and M. Boshta, *Mater. Sci. Semicond. Process.*, 109 (2020) 104944.
9. S.R. Nalage, M.A. Chougule, S. Sen, P.B. Joshi, and V.B. Patil, *Thin. Solid. Films.*, 520 (2012) 4835-4840.

10. A.S. Kondrateva, P.G. Bespalova, L.A. Filatov, E.M. Tanklevskaya, S.I. Pavlov, and S.E. Alexandrov, *Russ. J. Appl. Chem.*, 90 (6) (2017) 846-852.
11. S. Zhao, Y. Shen, P. Zhou, J. Zhang, W. Zhang, X. Chen, D. Wei, P. Fang, and Y. Shen, *Ceram. Int.,* 44 (1) (2018) 753-759.
12. L. Li, R. Chen, G. Jing, G. Zhang, F. Wu, and S. Chen, *Appl. Surf. Sci.*, 256 (14) (2010) 4533-4537.
13. T. Ibusuki, N. Izawa, and K. Takeuchi, *Chem. Lett.*, 49 (5) (1982) 629-630.
14. R.K. Gupta, K, Ghosh, and P.K. Kahol, *Physica. E. Low. Dimens. Syst. Nanostruct.*, 41 (4) (2009) 617-620.
15. L. Cattin, B.A. Reguig, A. Khelil, M. Morsli, K. Benchouk, and J.C. Bernede, *Appl. Surf. Sci.*, 254 (18) (2008) 5814-5821.
16. P.S. Patil and L.D. Kadam, *Appl. Surf. Sci.*, 199 (2002) 211-221.
17. M. Gardon and J.M. Guilemany, *J. Mater. Sci-Mater. El.*, 24 (5) (2013) 1410-1421.
18. D.G. Rickerby and A.N. Skouloudis, *Int. J. Nanotechnol.*, 11 (5/6/7/8) (2014) 583.
19. L. Wei, A. Chen, X. Lu, and J. Zhu, *J. Appl. Phys.*, 98 (2) (2005) 2268.
20. S.R. Lee, H.M. Kim, K. Char, J.H. Jang, M. Kim, M.R. Cho, Y.D. Park, R. Jung, D.C. Kim, and S. Seo, *Curr. Appl. Phys.*, 12 (2) (2012) 369-372.
21. G. Jiménez-Cadena, J. Riu, and F.X. Rius, *Analyst.*, 132 (2007) 1083-1099.
22. C. Ma, D. Zhao, H. Xia, F. Xia, Z. Ma, and T. Williams, *Int. J. Electrochem. Sci.*, 15 (2020) 4015.